SUPPLEMENTAL MATERIAL

Viscous-elastic dynamics of power-law fluids within an elastic cylinder

Evgeniy Boyko,[1] Moran Bercovici,[1] and Amir D. Gat[1]

[1]*Faculty of Mechanical Engineering, Technion - Israel Institute of Technology, Haifa, Israel*

CONTENTS

S.1. DERIVATION OF GOVERNING EQUATIONS FOR ELASTIC PROBLEM

We here provide an alternative derivation of the expressions for the normalized radial and axial deformations fields first obtained by Elbaz and Gat [1]. After introducing the governing equations for the elastic problem, (21)-(23), with the appropriate boundary conditions, (24)-(25), we define the stress resultants $\tilde{n}_{ij}$, $\tilde{n}_{ij} = \int_{\tilde{r}_c}^{\tilde{r}_c+\tilde{h}_m} \tilde{\sigma}_{ij} d\tilde{r}$, and the normalized internal and external stresses

$$\sigma_{rr} = \frac{\tilde{\sigma}_{rr}}{\tilde{\sigma}^*_{rr}}, \quad \sigma_{rz} = \frac{\tilde{\sigma}_{rz}}{\tilde{\sigma}^*_{rz}}, \quad \sigma_{zz} = \frac{\tilde{\sigma}_{zz}}{\tilde{\sigma}^*_{zz}}, \quad \sigma_{\theta\theta} = \frac{\tilde{\sigma}_{\theta\theta}}{\tilde{\sigma}^*_{\theta\theta}}, \quad p_e = \frac{\tilde{p}_e}{\tilde{p}^*}, \tag{S1}$$

where $\tilde{\sigma}^*_{ij}$ are characteristic stresses yet to be determined. Substituting (8) and (9) into (24), we obtain the normalized boundary conditions

$$\sigma_{rr}|_{r=1+\epsilon_3 d_r} = -p + 2\epsilon_1^2 \left|\frac{\partial u_z}{\partial r}\right|^{n-1} \frac{\partial u_r}{\partial r}, \tag{S2}$$

$$\sigma_{rz}|_{r=1+\epsilon_3 d_r} = \left|\frac{\partial u_z}{\partial r}\right|^{n-1} \left(\frac{\partial u_z}{\partial r} + \epsilon_1^2 \frac{\partial u_r}{\partial z}\right), \tag{S3}$$

$$\sigma_{rr}|_{r=1+\epsilon_3 d_r+\epsilon_2} = -p_e, \quad \sigma_{rz}|_{r=1+\epsilon_3 d_r+\epsilon_2} = 0, \tag{S4}$$

as well as appropriate characteristic stresses expressed as $\tilde{\sigma}^*_{rr} \sim \tilde{p}^*$ and $\tilde{\sigma}^*_{rz} \sim \tilde{\mu}_{eff}\left(\tilde{u}^*_z/\tilde{r}_c\right)^n \sim \epsilon_1\tilde{p}^*$. We note that while the characteristic radial length scale in the elastic problem is $\tilde{r}_c$, the appropriate length scale for the radial differential, $d\tilde{r}$, is the thickness of the cylinder, $\tilde{h}_m$. Therefore, performing order of magnitude analysis of (21) yields $\tilde{\sigma}^*_{zz} = \tilde{\sigma}^*_{\theta\theta} = \tilde{p}^*/\epsilon_2$ as well as the normalized governing equations

$$\frac{\partial}{\partial r}\left(r\sigma_{rr}\right) = \sigma_{\theta\theta} + O(\epsilon_1^2), \quad \frac{\partial}{\partial r}\left(r\sigma_{rz}\right) + \frac{\partial}{\partial z}\left(r\sigma_{zz}\right) = 0. \tag{S5}$$

Integrating (S5) with respect to r from 1 to $1+\epsilon_2$ and using (S2) and (S4) yields

$$p(z,t) - p_e - n_{\theta\theta}(z,t) \sim O(\epsilon_1^2), \tag{S6}$$

where $n_{\theta\theta} = \tilde{n}_{\theta\theta}/\tilde{n}^*_{\theta\theta} = \tilde{n}_{\theta\theta}/\tilde{\sigma}^*_{\theta\theta}\tilde{h}_m = \tilde{n}_{\theta\theta}/\tilde{r}_c\tilde{p}^*$. The force balance in the axial direction yields

$$n_{zz}(z,t) = \frac{1}{2}p(z,t), \tag{S7}$$

where $n_{zz} = \tilde{n}_{zz}/\tilde{n}^*_{zz} = \tilde{n}_{zz}/\tilde{\sigma}^*_{zz}\tilde{h}_m = \tilde{n}_{zz}/\tilde{r}_c\tilde{p}^*$. To express the resultants n_{zz} and $n_{\theta\theta}$ in terms of the radial and axial displacements, we normalize Hooke's law equations (23) based on the obtained characteristic values of $\tilde{\sigma}^*_{ij}$

$$\sigma_{zz} = \frac{\epsilon_2\tilde{E}}{\tilde{p}^*\left(1-\nu^2\right)}\left(\tilde{e}_{zz} + \nu\tilde{e}_{\theta\theta}\right), \quad \sigma_{\theta\theta} = \frac{\epsilon_2\tilde{E}}{\tilde{p}^*\left(1-\nu^2\right)}\left(\tilde{e}_{\theta\theta} + \nu\tilde{e}_{zz}\right). \tag{S8}$$

We apply the Kirchhoff hypothesis [see 2, 3] and describe the displacement field $\left(\tilde{d}_r, \tilde{d}_z\right)$ in terms of the radial $\bar{\tilde{d}}_r$ and axial $\bar{\tilde{d}}_z$ displacements of the mid-section $\tilde{r}_m = \tilde{r}_c + (\tilde{h}_m/2)$, denoted by tilded overbars,

$$\tilde{d}_z = \bar{\tilde{d}}_z - (\tilde{r} - \tilde{r}_m)\frac{\partial\tilde{d}_r}{d\tilde{z}}, \quad \tilde{d}_r = \bar{\tilde{d}}_r, \tag{S9}$$

and thus we can represent the strain as a function of the deformation by

$$\tilde{e}_{zz} = \frac{\partial\bar{\tilde{d}}_z}{d\tilde{z}} - (\tilde{r} - \tilde{r}_m)\frac{\partial^2\bar{\tilde{d}}_r}{d\tilde{z}^2}, \quad \tilde{e}_{\theta\theta} = \frac{\bar{\tilde{d}}_r}{\tilde{r}}. \tag{S10}$$

Substituting (S10) into (S8), integrating with respect to $\tilde{r}$, and normalizing yields the required resultants n_{zz} and $n_{\theta\theta}$ in terms of deformations

$$n_{zz} \sim \frac{\tilde{E}\epsilon_2\epsilon_3}{\tilde{p}^*\left(1-\nu^2\right)}\left(\nu\bar{d}_r + \frac{\partial\bar{d}_z}{\partial z}\right), \quad n_{\theta\theta} \sim \frac{\tilde{E}\epsilon_2\epsilon_3}{\tilde{p}^*\left(1-\nu^2\right)}\left(\bar{d}_r + \nu\frac{\partial\bar{d}_z}{\partial z}\right), \tag{S11}$$

as well as a relation between the characteristic radial deformation and characteristic pressure

$$\frac{\tilde{p}^*}{\epsilon_2 \tilde{E}} = \frac{\tilde{d}_r^*}{\tilde{r}_c} = \epsilon_3 \ll 1. \tag{S12}$$

Since $d_z = \bar{d}_z + O(\epsilon_1^2)$ and $d_r = \bar{d}_r$, substituting (S11) and (S12) into (S7) yields

$$\frac{\partial d_z}{\partial z} = \frac{1-\nu^2}{2} p(z,t) - \nu d_r. \tag{S13}$$

Finally, combining (S6) and (S11)-(S13), we obtain governing equations for the radial and axial deformations

$$d_r(z,t) = \left(1 - \frac{\nu}{2}\right) p(z,t) - p_e, \quad d_z(z,t) = \int_0^z \left[\left(\frac{1}{2} - \nu\right) p(z,t) + \nu p_e\right] dz. \tag{S14}$$

S.2. COMPARISON WITH ASYMPTOTIC SOLUTIONS

We here derive asymptotic solutions for the cases of constant and the oscillating inlet pressure, and compare them with the analytical and numerical results from Secs. IV B and IV C with the aim of estimating their validity. While in general, an asymptotic solution can be obtained by solving the PDEs (34) and (35), we show that when a similarity variable is identified, self-similar solutions can be obtained through the solution of a simpler ODE.

S.2.1. Constant inlet pressure

We here derive two different asymptotic solutions for the case of constant inlet pressure ($p_0 = 1$ and $p_i = 0$) and compare them with the exact solution (65). The corresponding leading-order solution is given in (60), whereas the first-order solution, obtained from (35), reads

$$p^{(1)}(z,t) = -\frac{z \mathrm{e}^{-z^2/4t}}{16\sqrt{\pi} t^{3/2}} \left(z^2 - 6t + 4t \ln(\pi t)\right). \tag{S15}$$

Since in this case the solution exhibits self-similarity with similarity variable (58) and satisfies the non-linear ordinary differential equation (61), an additional asymptotic solution may be found based on (61). Using (31) and defining the expansion $p_\xi(\xi) = p_\xi^{(0)}(\xi) + \varepsilon p_\xi^{(1)}(\xi) + O(\varepsilon^2)$, yields the leading- and the first-order corrections of (61) with appropriate boundary conditions

$$O(1): \quad \frac{d^2 p_\xi^{(0)}}{d\xi^2} + \frac{1}{2}\xi \frac{d p_\xi^{(0)}}{d\xi} = 0, \quad p_\xi^{(0)}(0) = 1, \quad p_\xi^{(0)}(\infty) = 0, \tag{S16}$$

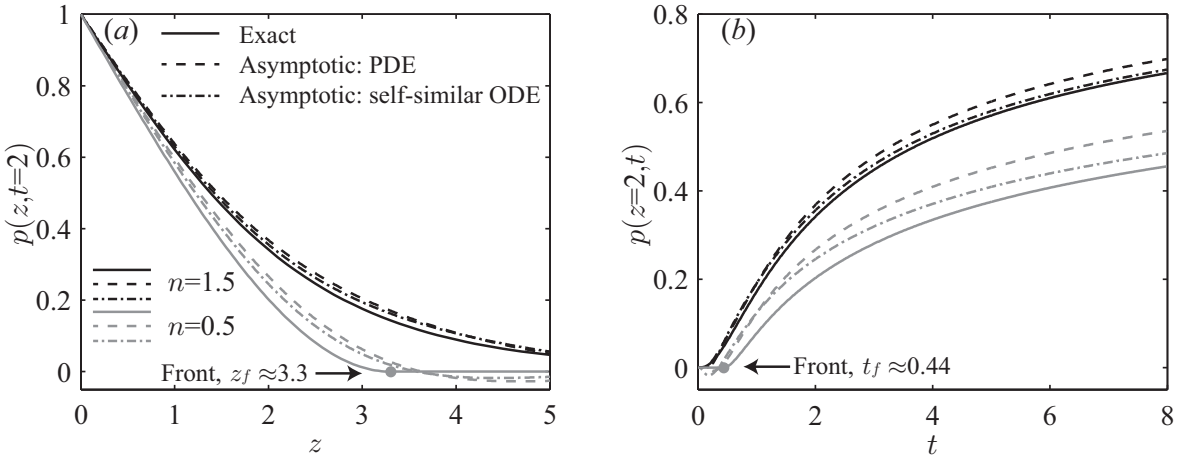

FIG. S1. Comparison between the exact solution and two asymptotic approximations for the case of constant pressure at the inlet. Solid lines correspond to exact solution, dashed lines correspond to asymptotic solution (S16), and dashed-dot lines correspond to self-similar asymptotic solution (S18). (a) Pressure versus axial coordinate for $t = 2$. (b) Pressure at $z = 2$ as function of time. Solid and dashed lines correspond to $t = 0.1$ and $t = 1.0$, respectively. Black lines represent a shear-thickening fluid ($n = 1.5$), gray lines represent a shear-thinning fluid ($n = 0.5$), and thick gray dots show the front.

and

$$O(\varepsilon): \quad \frac{d^2 p_\xi^{(1)}}{d\xi^2} + \frac{1}{2}\xi \frac{dp_\xi^{(1)}}{d\xi} = \frac{1}{4}\xi \frac{dp_\xi^{(0)}}{d\xi}\left(3 + 2\ln\left(-\frac{dp_\xi^{(0)}}{d\xi}\right)\right), \quad p_\xi^{(1)}(0) = p_\xi^{(1)}(\infty) = 0. \tag{S17}$$

The solution of (S16) and (S17) in terms of the similarity variable ξ is

$$p_\xi^{(0)}(\xi) = \operatorname{erfc}\left(\frac{\xi}{2}\right), \quad p_\xi^{(1)}(\xi) = -\frac{\xi e^{-\xi^2/4}}{16\sqrt{\pi}}\left(\xi^2 - 6 + 4\ln\pi\right), \tag{S18}$$

while the corresponding solution in terms of z and t is obtained by substituting $\xi = zt^{-n/n+1}$ into (S18).

In Fig. S1, we compare the exact (solid lines) and two different asymptotic (dashed and dashed-dot lines) solutions for the pressure field resulting from constant pressure at the inlet, for $n = 0.5, 1.5$. Figure S1(a) presents the pressure distribution as function of the axial coordinate z for $t = 2$, whereas Fig. S1(b) shows the pressure variation with time at $z = 2$. The dashed lines represent the asymptotic solution (S15), and the dashed-dot lines represent the self-similar asymptotic solution (S18). As expected, Figure S1 indicates that the self-similar asymptotic solution (S18) shows better agreement with the exact solution as compared to (S15).

S.2.2. Oscillatory inlet pressure

We here determine a closed-form asymptotic solution for the case of oscillating pressure at the inlet and then compare it with the numerical solution of (28). For simplicity and clarity, we focus on the case of $\omega = 2\pi$. The leading-order asymptotic solution is given in (71), and by substituting (71) into the right-hand-side of (35) the first-order solution is obtained from

$$\frac{\partial p^{(1)}}{\partial t} - \frac{\partial^2 p^{(1)}}{\partial z^2} = \pi \mathrm{e}^{-\sqrt{\pi}z} \left[-2 + 2\sqrt{\pi}z - \ln\left(\pi\left(1 + \sin\left(2\sqrt{\pi}z - 4\pi t\right)\right)\right)\right] \mathrm{Im}\left\{\mathrm{e}^{i\left(2\pi t - \sqrt{\pi}z\right)}\right\}. \tag{S19}$$

Substituting $p^{(1)}(z,t) = \pi \mathrm{e}^{-\sqrt{\pi}z} \mathrm{Im}\left\{\mathrm{e}^{i\left(2\pi t - \sqrt{\pi}z\right)} F^{(1)}(z,t)\right\}$ into (S19) yields

$$\frac{\partial F^{(1)}}{\partial t} + 2\sqrt{\pi}\,(1+i)\,\frac{\partial F^{(1)}}{\partial z} - \frac{\partial^2 F^{(1)}}{\partial z^2} = -2 + 2\sqrt{\pi}z - \ln\left(\pi\left(1 + \sin\left(2\sqrt{\pi}z - 4\pi t\right)\right)\right). \tag{S20}$$

Employing the superposition principle, the solution of (S20) can be written in terms of Green's function as the sum of three contributions resulting from the source terms of (S20)

$$F_1^{(1)}(z,t) = -2\int_0^t \int_0^\infty G\left(z, z', t - t'\right) dz' dt', \tag{S21a}$$

$$F_2^{(1)}(z,t) = 2\sqrt{\pi}\int_0^t \int_0^\infty z' G\left(z, z', t - t'\right) dz' dt', \tag{S21b}$$

$$F_3^{(1)}(z,t) = -\int_0^t \int_0^\infty \ln\left(\pi\left(1 + \sin\left(2\sqrt{\pi}z - 4\pi t\right)\right)\right) G\left(z, z', t - t'\right) dz' dt' \tag{S21c}$$

where $G\left(z, z', t\right)$ is the Green's function [4]

$$G\left(z, z', t\right) = \frac{1}{\sqrt{4\pi t}} \exp\left(-\sqrt{\pi}\,(1+i)\,(z' - z) - 2\pi i t\right)\left\{\mathrm{e}^{-\frac{(z-z')^2}{4t}} - \mathrm{e}^{-\frac{(z+z')^2}{4t}}\right\}, \tag{S22}$$

and then the solution of (S19) reads

$$p^{(1)}(z,t) = \pi \mathrm{e}^{-\sqrt{\pi}z} \mathrm{Im}\left\{\mathrm{e}^{i\left(2\pi t - \sqrt{\pi}z\right)}\left(F_1^{(1)}(z,t) + F_2^{(1)}(z,t) + F_3^{(1)}(z,t)\right)\right\}. \tag{S23}$$

The first two contributions (S21a) and (S21b) can be obtained analytically,

$$\begin{aligned} F_1^{(1)}(z,t) =& \frac{1}{4\sqrt{\pi}}\left\{(1-i)\left((2+2i)\sqrt{\pi}t + z\right)\left(-1 + \mathrm{e}^{(2+2i)\sqrt{\pi}z}\mathrm{erfc}\left(\frac{(2+2i)\sqrt{\pi}t + z}{2\sqrt{t}}\right)\right)\right. \\ &\left. + \left(4\sqrt{\pi}t - (1-i)z\right)\mathrm{erf}\left(\frac{(2+2i)\sqrt{\pi}t - z}{2\sqrt{t}}\right)\right\}, \end{aligned} \tag{S24}$$

and

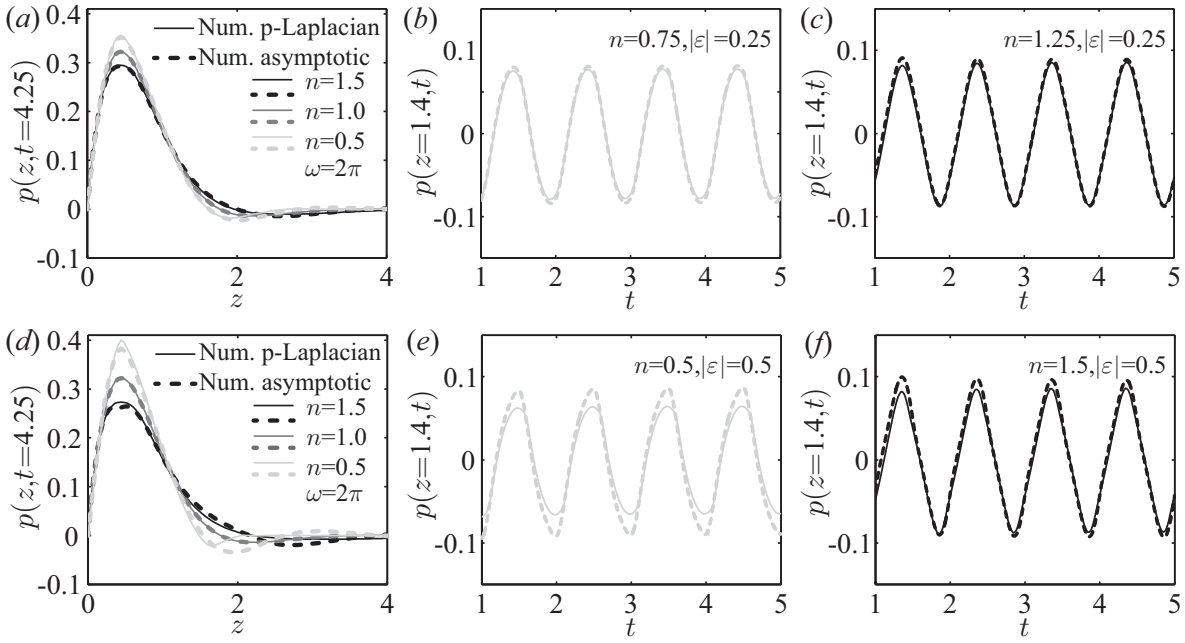

FIG. S2. Comparison between numerical solutions the p-Laplacian equation (28) (solid lines) and the linear asymptotic equations (dashed lines), for the case of oscillatory pressure at the inlet. Black lines represent a shear-thickening fluids, dark gray lines represent a Newtonian fluids and light gray lines represent a shear-thinning fluids. (a) Pressure versus axial coordinate at $t = 4.25$ for $n = 0.75,\ 1,\ 1.25$. (b,c) Pressure as a function of time at $z = 1.4$ for $n = 0.75$ and $n = 1.25$, respectively. (d) Pressure versus axial coordinate at $t = 4.25$ for $n = 0.5,\ 1,\ 1.5$. (e,f) Pressure as a function of time at $z = 1.4$ for $n = 0.5$ and $n = 1.5$, respectively.

$$F_2^{(1)}(z,t) = \frac{1}{8\sqrt{\pi}}\left\{-2iz\left(1+(1+i)\sqrt{\pi}z\right)+(-4+4i)\,\mathrm{e}^{-\frac{\left((2+2i)\sqrt{\pi}t-z\right)^2}{4t}}z\sqrt{t}+\right.$$
$$+\left(iz+(1-i)\sqrt{\pi}\left((2+2i)\sqrt{\pi}t+z\right)^2\right)\mathrm{e}^{(2+2i)\sqrt{\pi}z}\mathrm{erfc}\left(\frac{(2+2i)\sqrt{\pi}zt+z}{2\sqrt{t}}\right)+$$
$$\left.+\left(iz-(1-i)\sqrt{\pi}\left((2+2i)\sqrt{\pi}t-z\right)^2\right)\mathrm{erfc}\left(\frac{(2+2i)\sqrt{\pi}zt-z}{2\sqrt{t}}\right)\right\}. \qquad \text{(S25)}$$

We were not able to obtain an explicit analytical expression for (S21c) and thus we solved the linear parabolic equation (S19) numerically. Figure S2 presents a comparison between the numerical solution of the original p-Laplacian equation (28) (solid lines) and the numerical solution of the asymptotic equations (dashed lines), (34) and (35). Figures S2(a) and S2(d) show the resulting pressure distribution versus axial coordinate at $t = 4.25$ for the cases of $|\varepsilon| = 0.25$ ($n = 0.75,\ 1.25$) and $|\varepsilon| = 0.5$ ($n = 0.5,\ 1.5$), whereas Figs. S2(b,c) and S2(e,f) show the corresponding pressure as a function of time at $z = 1.4$. For small values of $|\varepsilon|$, there is good agreement

between two numerical solutions, indicating the applicability of the asymptotic equations in this case. However, we observe significant differences between the two solutions as $|\varepsilon|$ increases.

S.3. NUMERICAL SECOND-ORDER SCHEME FOR P-LAPLACIAN EQUATION

In this section, we present the derivation of a finite-difference numerical method that solves the unforced p-Laplacian equation (28) for both shear-thinning ($n < 1$) and shear-thickening ($n > 1$) fluids. For convenience, we rewrite (28) in the conservative form

$$\frac{\partial p}{\partial t} = \frac{\partial F}{\partial z}, \tag{S26}$$

introducing the function $F(z,t)$ defined as

$$F \equiv \left|\frac{\partial p}{\partial z}\right|^{\frac{1}{n}-1}\frac{\partial p}{\partial z} = \operatorname{sgn}\left(\frac{\partial p}{\partial z}\right)\left|\frac{\partial p}{\partial z}\right|^{\frac{1}{n}} = \operatorname{sgn}\left(\frac{\partial p}{\partial z}\right)\left(\left(\frac{\partial p}{\partial z}\right)^2\right)^{\frac{1}{2n}}. \tag{S27}$$

While analytical solutions (see Sec. IV) are available for a semi-infinite domain, we are here interested in solving (S26) on a finite domain $(0, L)$ subjected to Dirichlet boundary conditions at $z = 0$ and $z = L$

$$p(0,t) = p_{inlet}(t), \quad p(L,t) = 0, \tag{S28}$$

with initial condition $p(z,0) = 0$.

Let p_i^m denote the approximation to $p((i-1)\,\Delta z, (m-1)\,\Delta t)$ on the uniform grid $z_i = (i-1)\,\Delta z$, where $\Delta z = L/\,(N-1)$ is a spatial interval and N is the total number of spatial grid points. Subscript i ($i = 1, ..., N$) denotes indices in the $\hat{\boldsymbol{z}}$ direction, and superscript m denotes time steps of size Δt. The conservative semi-discrete form of (S26) is

$$\frac{\partial p_i}{\partial t} = \frac{F_{i+1}^m - F_{i-1}^m}{2\Delta z}, \tag{S29}$$

which is second-order accurate in space. The function F_i^m can be written in second-order discrete form as

$$F_i^m = \begin{cases} \operatorname{sgn}\left(\frac{p_{i+1}^m - p_{i-1}^m}{2\Delta z}\right)\left(\left(\frac{p_{i+1}^m - p_{i-1}^m}{2\Delta z}\right)^2\right)^{\frac{1}{2n}} & i = 2, ...N-1 \\ \operatorname{sgn}\left(\frac{-3p_1^m + 4p_2^m - p_3^m}{2\Delta z}\right)\left(\left(\frac{-3p_1^m + 4p_2^m - p_3^m}{2\Delta z}\right)^2\right)^{\frac{1}{2n}} & i = 1 \\ \operatorname{sgn}\left(\frac{3p_N^m - 4p_{N-1}^m + p_{N-2}^m}{2\Delta z}\right)\left(\left(\frac{3p_N^m - 4p_{N-1}^m + p_{N-2}^m}{2\Delta z}\right)^2\right)^{\frac{1}{2n}} & i = N \end{cases}, \tag{S30}$$

where from (S28) we have $p_1^m = p_{inlet}^{(m-1)\Delta t}$ and $p_N^m = 0$.

After evaluating (S30) for time step m, we integrate (S26) to determine p_i^m in the next time step. To initiate the solution (for $m = 1$), we use the first-order Euler method:

$$p_i^2 = p_i^1 + \Delta t \frac{F_{i+1}^1 - F_{i-1}^1}{2\Delta z}, \tag{S31}$$

while in all subsequent time steps (for $m \geq 2$) we use the second-order Adams-Bashforth method:

$$p_i^{m+1} = p_i^m + \frac{3}{2}\Delta t \frac{F_{i+1}^m - F_{i-1}^m}{2\Delta z} - \frac{1}{2}\Delta t \frac{F_{i+1}^{m-1} - F_{i-1}^{m-1}}{2\Delta z}. \tag{S32}$$

Thus, the scheme is formally second-order accurate in both time and space, and has a truncation error of $O\left((\Delta z)^2, (\Delta t)^2\right)$ (except for the first time step that involves the use of first-order Euler integration).

---

[1] S. B. Elbaz and A. D. Gat, Dynamics of viscous liquid within a closed elastic cylinder subject to external forces with application to soft robotics, J. Fluid Mech. **758**, 221 (2014).

[2] E. Ventsel and T. Krauthammer, *Thin plates and shells: theory: analysis, and applications* (CRC Press, 2001).

[3] J. N. Reddy, *Theory and analysis of elastic plates and shells* (CRC Press, 2006).

[4] A. D. Polyanin, *Handbook of Linear Partial Differential Equations for Engineers and Scientists* (CRC Press, 2001).